

Subarcsec structures in the double nucleus of NGC 6240 disclosed with HST at 370, 430 and 500 nm[★]

P. Rafanelli^{2,7}, H. Schulz^{3,4,5}, C. Barbieri^{1,2}, S. Komossa^{4,6}, U. Mebold³, A. Baruffolo^{2,8}, and M. Radovich²

¹ Member FOC Investigation Definition Team

² Department of Astronomy, University of Padova, Vicolo Osservatorio 5, I-35122 Padova, Italy

³ Radioastronomisches Institut, Universität Bonn, Auf dem Hügel 71, D-53121 Bonn, Germany

⁴ Astronomisches Institut der Ruhr-Universität, D-44780 Bochum, Germany

⁵ Institut für Astronomie und Astrophysik, Universität Tübingen, Waldhäuser Str. 64, D-72076 Tübingen, Germany

⁶ Max-Planck-Institut für Extraterrestrische Physik, Postfach 1603, D-85740 Garching, Germany

⁷ Astrophysikalisches Institut Potsdam, An der Sternwarte 16, D-14482 Potsdam, Germany

⁸ Osserratorio Astronomico di Padova, Vicolier Osservatorio 5, I-35122 Padova, Italy

Received 25 June 1996 / Accepted 20 January 1997

Abstract. We present an analysis of three medium band width (FWHM $\sim 400 - 450 \text{ \AA}$) images of the nuclear region of NGC 6240 taken with the pre-COSTAR Faint Object Camera (FOC) on board of the *Hubble Space Telescope*. The first filter band comprises the [OII] $\lambda 3727$ doublet, the second measures the blue continuum around 4400 \AA and the third includes $H\beta + [\text{OIII}]\lambda\lambda 4959, 5007$. The images show that the apparent two galactic nuclei B (north) and A (south) identified from the ground consist of compact substructures on the tenth-arcsec scale plus faint extended emission on the arcsec scale. Within a diameter of $0''.26$ ($\sim 120 \text{ pc}$), most compact features exhibit a summed line luminosity $L([\text{OIII}] + H\beta)$ in the range $10^{39} - 10^{40} \text{ erg s}^{-1}$ which is comparable to that of giant HII regions.

Although the data are not complete enough for a direct decomposition into line and continuum flux, probable solutions yield a LINER like [OII]/[OIII]/ $H\beta$ line ratio for the northern compact subcomponent B1. In the southern nucleus A the faint subcomponents A2 and A3 can be classified as LINER like if they are more strongly reddened than B1 or as HII-region like if not.

The brightest southern compact component A1, however, exhibits line ratios that are typical of (i) a Seyfert galaxy or (ii) a high-excitation HII region. This leads to the interesting alternative that there is either (i) a hidden AGN (which is in accord with recent ASCA observations) or (ii) a hidden cluster of young massive stars. The second possibility would imply localized ongoing star formation within an environment whose visible light is dominated by radiation from older stellar populations. However, considering recent models for fast autoionizing

shocks computed by Dopita & Sutherland (1995), A1 might also represent a shock-plus-precursor region.

Key words: galaxies: active – galaxies: interactions – galaxies: nuclei – galaxies: individual: NGC 6240

1. Introduction

The peculiar galaxy NGC 6240 shows conspicuous loops and tails considered as signs of gravitational interaction (Zwicky et al. 1961; Fosbury & Wall 1979), two apparent nuclei (Fried & Schulz 1983) and an extraordinary luminosity in the infrared ($\sim 10^{12} L_{\odot}$; Wright et al. 1984). Its mid infrared radiation is strongly concentrated in the nuclear region as is evidenced by the $10-32 \mu\text{m}$ radiation 91% of which arises within an aperture of $5''.7$ (Wynn-Williams & Becklin 1993).

The ultimate source of the nuclear IR radiation has not yet been unambiguously identified but might be reprocessed energy from the merging process (Harwit et al. 1987), ordinary starlight (Thronson et al. 1990), a super starburst (Joseph et al. 1984, Joseph & Wright 1985) or a dust shrouded quasar (de Poy et al. 1986; Sanders et al. 1988). The enigma of the primary power source provided one of the motivations to carry out *Hubble Space Telescope* (HST) observations, which were first conducted by Barbieri et al. (1993; hereafter paper I) who published an image taken with the FOC through the medium band filter F372M (peak wavelength $\lambda_0 = 3710 \text{ \AA}$, FWHM $\Delta\lambda = 412 \text{ \AA}$ of combined filter, telescope and FOC response function; c.f. Paresce 1990).

The FOC image revealed several compact knots within the apparent double nucleus on scales down to $0''.1$. While the northern nucleus contains just one compact concentration, at

Send offprint requests to: P. Rafanelli

[★] Based on observations with the NASA/ESA *Hubble Space Telescope*, obtained at the Space Telescope Science Institute, which is operated by AURA, Inc., under NASA contract NAS 5-26555

least three subarcsecond knots were discerned within the southern nucleus. Notable diffuse emission on a scale of $\sim 1''$ is present in both nuclei as well. The roundish appearance of the southern nucleus on groundbased images turned out to be due to the convolution of a seeing disk with the sum of the compact knots and the extended emission. This was demonstrated by a convolution experiment with the HST image which even showed that the steepening of the brightness gradient seen from the ground on the eastern side of the nucleus has to be traced back to the asymmetric location of the compact sources relative to the underlying extended source.

In the present paper we add to the F372M image (shown in Fig. 1) additional FOC/HST observations. The new data were taken in blue continuum light (around 4400 Å) as well as through a medium band filter that includes H β and [OIII] λ 5007.

As in paper I, we assume a distance $d = 96$ Mpc or $m - M = 35^m$ yielding a flux–luminosity conversion factor $4\pi d^2 = 1.1 \cdot 10^{54}$ cm² and a linear scale of 460 pc arcsec⁻¹ parallel to the plane of the sky. The sum of the lines [OII] λ 3726 and λ 3729 is abbreviated by [OII] λ 3727.

2. Observations and data reductions

The new images were obtained on 1993 April 15/16 employing the filters F437M ($\lambda_0 = 4290$ Å, $\Delta\lambda = 446$ Å) and F502M ($\lambda_0 = 4920$ Å, $\Delta\lambda = 422$ Å) and the FOC in the f/96, 512 × 512 mode with a field size of 11'' × 11'' leading to an effective pixel size of 0''.022 px⁻¹. The observation through each filter was split into five exposures each of 596.75 sec duration. After the usual pipeline correction for geometrical distortion the frames were coadded and then deconvolved by performing fifteen iterations with Lucy's (1974) algorithm. The iterations had to be stopped because otherwise spurious background features were overamplified.

For the deconvolution we utilized normalized point spread functions (PSF) derived from 496 sec exposures of the standard star BPM 16274 (frames F437M-A (Prop 3929) and F502M-A (Prop 3929) from the F/96 PSF directory for the day 323 Secondary Mirror Position after day 390).

Gray tone reproductions of the old and new deconvolved images are given in Figs. 1–3. Since the position angle of the spacecraft varied between the exposures the field of the sky observed is not the same in all frames. The figures show the fields common to the three frames after frame rotation. In paper I we labeled image structures by A to E. The present work deals only with the prominent sources B and A (the two nuclei) because, due to a drop in the FOC sensitivity features C to E are too faint in the new images or not covered.

The lack of stars in the field does not allow to align the images independently from the structures to be measured. As the best compromise, in each image we determined the centroid of the conspicuous knot B1 (FWHM 0''.14) in the northern nucleus B and shifted the F372M and F437M frames to the pixel scale of the F502M frame.

This method assumes that the northern nucleus has a constant position in the wavelength range 3500 Å to 5200 Å. Reas-

suring evidence for this assumption comes from the fact that in *ground-based* B, V, R, z filter images the position of the northern nucleus is the same within $\leq 0''.12$ (Schulz et al. 1993). On our HST images the similarity of the compact structure B1 with its southern slightly diffuse extension in all three images even suggests that its position on the three frames should coincide within 0''.05 or better (Figs. 4–6).

3. Photometric calibration

The old F372M (“U”) image was calibrated in paper I by using groundbased multiaperture U-photometry given in Thronson et al. (1990). This calibration alone does not allow a separation of the continuum from the [OII] λ 3727 emission-line doublet.

In order to decompose lines and continuum we also calibrated all three images via a comparison with the spectrum scan observed by Fosbury & Wall (1979; FW79). A counterpart of their 18 arcsec² observing aperture (3'' × 6'') was mapped onto the image and the integrated counts were matched with the mean spectral flux derived by convolving the spectrophotometric scan with the appropriate effective filter response curves from the FOC handbook (Paresce 1990). This procedure led to scaling factors that, when applied to the images, put them on the same relative scale consistent with the groundbased spectrophotometry and photometry.

In each filter band we also extracted the effective percentage of line flux from the FW79 spectrum which is seen by the OTA–FOC–filter combination. [OII] λ 3727 contributes 14% of the continuum in the F372M filter, and [OIII] λ 4959 + λ 5007 + H β amounts to 4.5% of the continuum in the F502M filter. According to the spectrum, the F437M band appears to contain pure continuum light. Therefore the F372M frame was appropriately scaled to the continuum level underlying the lines in the other bands. Line fluxes were derived in selected apertures after having subtracted the scaled continuum frames from the F502M and F372M frames. This continuum subtraction procedure would be correct provided the slope of the continuum between 3500 and 5200 Å does not vary over the image. However, in fact the continuum slope can vary due to variable amounts of extinction. The corresponding effects will be discussed in Sect. 5.

4. Morphology

The nuclei B (north) and A (south) contain extended emission plus compact substructures. Although on a faint level, and therefore spurious in details, with suitably chosen isophotes the shape of the *extended* structures ($\sim 1''$) is strikingly similar on the three images. Faint emission extends to the south and west of the compact northern “subnucleus” B1 (Figs. 4–6). Low-surface brightness emission also spreads out to the west of the southern compact components and is accompanied by a ‘nose’ to the NE. An absorption or low-emission ‘channel’ lies between the northern and southern emission structures.

To the apparently compact structures in the southern nucleus A1, A2 and A3 we add here a fourth component A4 which can

be recognized as a separate knot in image F502M (Fig. 6). In Table 1 we give the positions of the subcomponents relative to B1 in an $x-y$ coordinate system (positive x : eastwards; positive y : north).

The next conspicuous component, A1 (Figs. 4–6), can be identified in all three images (see the markings in Figs. 4–6). The situation is different for component A2 which is still apparent in the pure continuum image F437M (Fig. 5) but has no compact counterpart in the F502M image (Fig. 6) that includes $H\beta$ and $[OIII]$. In this image A1 shows only a slight extension towards the position of A2. The absence of A2 in the F502M frame cannot be attributed to extinction (which would have its strongest obscuring effect in F372M) but marks an outstandingly blue feature.

A3 cannot be discerned as a component in Figs. 5 and 6 but is anyway weak even on its defining image (Fig. 4 and see paper I, Fig. 2b). We nevertheless use it for photometric measurements in the next section.

As a compact knot, A4 is only well defined in the F502M frame (Fig. 6); a corresponding diffuse northwest appendix may also be present on F437M (Fig. 5). The unambiguously clear appearance of A4 on the “reddest” frame is consistent with the presence of a strong extinction effect. This is further supported by the fact that A4 lies in the zone between the two nuclei where a large molecular cloud complex was detected (Herbst et al. 1990; van der Werf et al. 1993; and cf. Schulz et al. 1993).

There is another faint knot north of A4 visible on the F372M and F437M frames but absent on our ‘red’ frame F502M. Here blue scattered light, low-excitation gas dominated by $[OII]\lambda 3727$ or a blue stellar population could be involved while a pure extinction effect appears to be ruled out.

Since only the strong knots B1 and A1 coincide on all three images, the conditions in the southern nucleus cannot be as uniform as might be imagined from the smeared out groundbased spectroscopy as e.g. suggested by spectra shown in Keel (1990).

5. Photometry

5.1. Direct results (without correction for extinction variations)

As described in Sect. 3 we deduced fluxes of the blue $[OII]$ doublet as well as of $[OIII]+H\beta$ in circular apertures (Table 1). Possible systematic errors in these numbers relative to each other induced by patchy extinction will be discussed in Sect. 5.2. Counting statistics alone makes these line fluxes 10–30% uncertain (the two values labeled by ‘:’ provide order of magnitude estimates because they are based only on few counts). The most severe uncertainty, in particular for small apertures, arises by the subtraction procedure of two fluctuating frames. Line ratios based on aperture diameters $\geq 0''.26$ should nevertheless be accurate within a factor of two if the error is dominated by the statistical fluctuations.

Following Baldwin et al. (1981; BPT), further diagnostics is given by the $[OII]\lambda 3727/[OIII]\lambda 5007$ (hereafter $[OII]/[OIII]$) ratio which can be derived from the measured $[OII]/([OIII]+H\beta)$

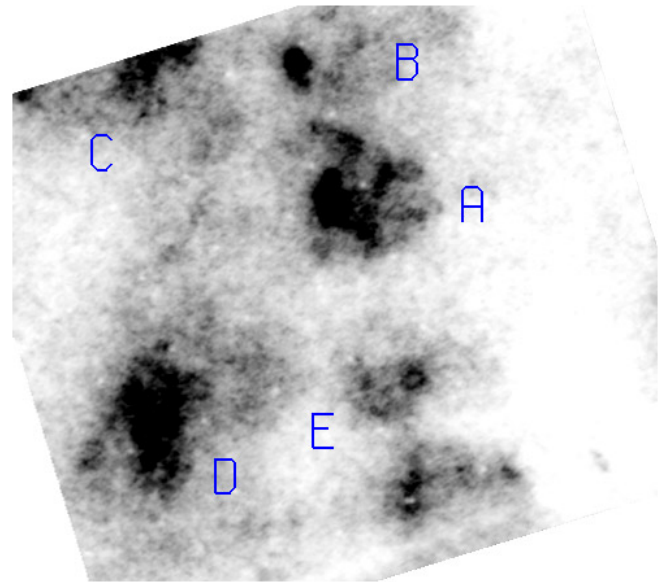


Fig. 1. F372M frame tilted so that east=left and north=up. The filter encloses the $[OII]\lambda 3727$ emission-line doublet and the UV continuum around 3700 \AA . The total exposure time is one hour with the *Faint Object Camera* of the *Hubble Space Telescope*. Structural features are marked: B northern nucleus, A southern nucleus (B and A are $2''$ apart); C, D, E extended emission features

values if $[OIII]/H\beta$ is assumed. In order to bracket the range covered by the majority of emission-line regions we assumed the three line ratios $[OIII]\lambda 5007/H\beta = 1.0, 3.12, 10.0$ (0.0, 0.5, 1.0, respectively, on a logarithmic scale).

In this way we obtained a set of three individual $[OII]/[OIII]$ ratios for each measured value of $[OII]/([OIII]+H\beta)$. The results derived for regions A1, A3, A4 and B1 and an aperture diameter of $0''.26$ are displayed in Fig. 7 (values for other apertures do not strongly differ). The BPT ranges for low to high-excitation HII regions, planetary nebulae, Seyferts and LINERs are drawn as well. We then adopt as the most plausible $[OIII]/H\beta$ ratio the value that leads to the closest match with one of the regions of known object classes yielding $5007/H\beta \approx 10$ for A1, a range 3–10 for A3 or A4 and about 1–3 for B1.

We know from the spectrum of FW79 that the sum of the compact and extended emission over $3'' \times 6''$ is LINER like and it is interesting whether the morphologically conspicuous components deviate from this. Fig. 7 shows that the northern compact nucleus B1 is indeed consistent with being LINER like (or a low-excitation HII region), but A3 and A4 tend to a higher-excitation HII region or could even be AGN like. However, a rather peculiar line-ratio arises for the strongest southern compact component, A1, which lies in the region of planetary nebulae with an $[OII]/[OIII]$ ratio drastically below that of AGN.

Table 1. Line fluxes $f([\text{OII}]3727)$ and $f([\text{OIII}]4959,5007+\text{H}\beta)$ extracted from the images by subtracting a continuum frame calibrated with a spatial average (in $\text{ergs s}^{-1} \text{cm}^{-2}$); individual fluxes will be larger or smaller in case of local deviations from the average extinction (see Sect. 5.2)

Component	Aperture diam.	Δx	Δy	M_U	$f([\text{OII}]3727)$	$f([\text{OIII}]+\text{H}\beta)$
B1	0''.26	0''.00	0''.00	-13 ^m .7	$2.62 \cdot 10^{-15}$	$2.85 \cdot 10^{-15}$
	0''.52				$4.50 \cdot 10^{-15}$	$7.50 \cdot 10^{-15}$
A1	0''.22	-0''.62	-2''.00	-12 ^m .1	$3.70 \cdot 10^{-17}$:	$1.05 \cdot 10^{-14}$
	0''.26				$7.95 \cdot 10^{-17}$:	$1.28 \cdot 10^{-14}$
	0''.36				$1.28 \cdot 10^{-16}$	$1.68 \cdot 10^{-14}$
A2	0''.22	-0''.44	-2''.16	-12 ^m .1		$1.43 \cdot 10^{-15}$
	0''.26					$2.67 \cdot 10^{-15}$
	0''.36					$5.93 \cdot 10^{-15}$
A3	0''.22	-0''.75	-2''.35		$5.04 \cdot 10^{-16}$	$3.40 \cdot 10^{-15}$
	0''.26				$5.75 \cdot 10^{-16}$	$4.26 \cdot 10^{-15}$
	0''.36				$7.54 \cdot 10^{-16}$	$6.61 \cdot 10^{-15}$
A4	0''.22	-0''.84	-1''.61		$2.15 \cdot 10^{-16}$	$2.73 \cdot 10^{-15}$
	0''.26				$2.91 \cdot 10^{-16}$	$3.20 \cdot 10^{-15}$
	0''.36				$5.44 \cdot 10^{-16}$	$4.17 \cdot 10^{-15}$

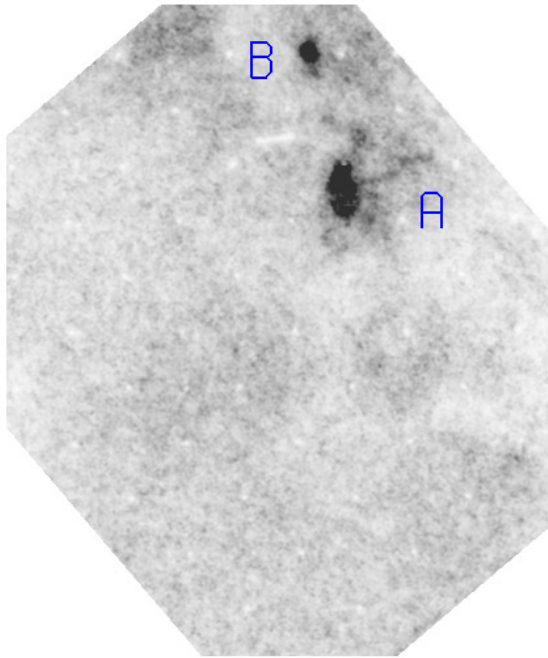


Fig. 2. As in Fig. 1 but through filter F437M (blue continuum)

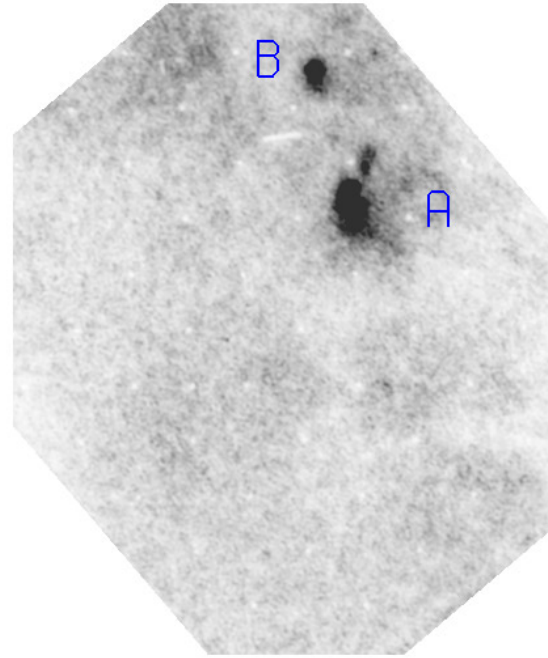


Fig. 3. As in Fig. 1 but through filter F502M (covering $\text{H}\beta + [\text{OIII}]\lambda\lambda 4959, 5007$ and continuum underneath)

5.2. Inclusion of above-average extinction in the southern nucleus

So far, we did not include any correction for extinction by dust although several authors (FW79, DePoy et al. 1986, Keel 1990, Thronson et al. 1990) agree upon $A_V = 3^m - 4^m$ in the nuclear region. With a standard reddening law (Draine 1989), $A_V = 4^m$ leads to a logarithmic difference of 0.68 in the 3727/5007 line ra-

tio which is indicated in Fig. 7 by the upper (small) arrow. Shifting the A1 data points by this amount will, however, still leave A1 at rather high excitation. Since extinction may be patchy it is unclear by which amount the other components need extinction corrections. The 4^m arrow would shift A3 and A4 into the LINER regime and B1 would become a LINER of rather low excitation.

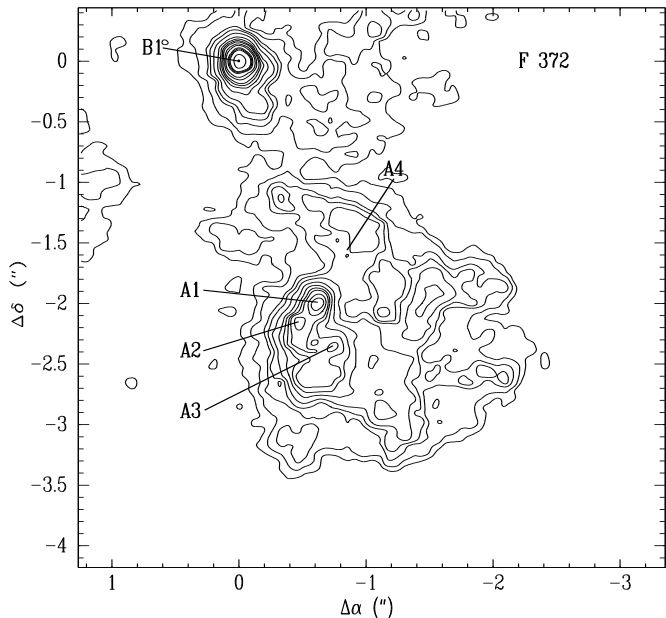


Fig. 4. Zoom from Fig. 1 showing the structure of the nuclei through the F372M filter. Subcomponents B1, A1, A2 and A3 (and A4; see Fig. 6) are marked

Extinction might have influenced the above deduced line ratios by another effect as well. In Sect. 3 we pointed out that the validity of the so far employed continuum subtraction rests on the constancy of the continuum gradient, i.e. the ratio between the continuum below a line and that measured in the F437M filter must be constant over the subtracted field. This constancy is only secured if the stellar population and the amount of extinction is everywhere the same. Our above procedure employed the continuum gradient from FW79 which gives an average over the central 18 arcsec².

In case of local above-average extinction we would subtract too low of a continuum value around 5000 Å and a too large value at 3700 Å, thereby artificially boosting the deduced [OIII]λ5007 flux and lowering [OII]λ3727. The groundbased multiaperture broad-band photometry of the two nuclei given in Thronson et al. (1990; their Table 2) indeed shows the southern nucleus A to be redder than the northern nucleus B. This is very likely due to stronger extinction.

The situation is displayed in Fig. 8 where the magnitude difference of the two nuclei is given together with extinction corrections for different geometrical extinction models: (i) the classical screen formula $I_\lambda = I_{\lambda_0} \exp(-\tau_\lambda)$ with a visual extinction $A_V = 1.086\tau_V = 1^m$; a model for homogeneously distributed emitters in a plane parallel layer given by $I_\lambda = I_{\lambda_0}(1 - \exp(-\tau_\lambda))/\tau_\lambda$ (Thronson et al. 1990) with either (ii) $\tau_V = 1.0$ or (iii) $\tau_V = 1.5$. The last model leads to a U magnitude difference of the two nuclei comparable to that in the H and K band. The screen model (i) would lead to an unphysically high ultraviolet flux of A (Fig. 9).

Since we are interested in the slope of the *stellar* continuum, the extinction law for emitters distributed in a homogeneous slab

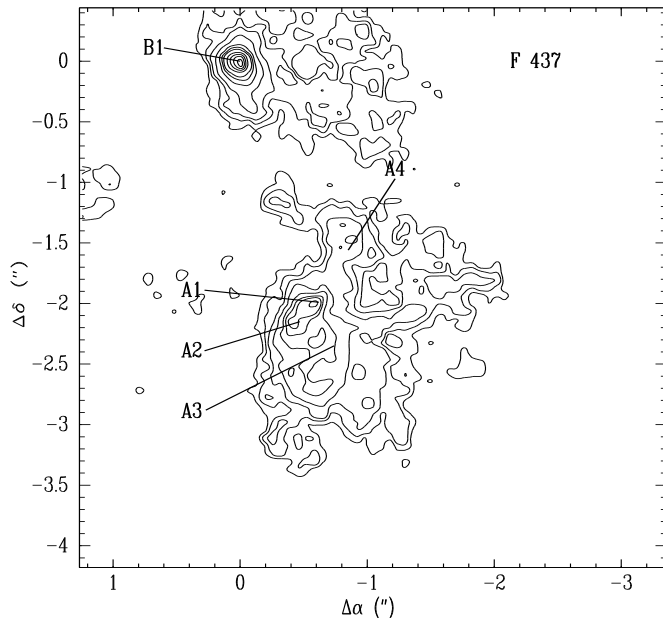


Fig. 5. Zoom from Fig. 2 showing the structure of the nuclei in blue continuum light (F437M)

(models (ii) or (iii)) should be better suited than the screen model (i) (Thronson et al. 1990). As shown in Fig. 9, the homogeneous model (iii) appears to be more plausible with regard to the UV excess.

The effect on the 3727/5007 line ratio is about $\Delta \log \approx 1$ for model (iii), shown by the lower arrow in Fig. 7, which is appreciably more than directly correcting the line ratios for an extinguishing screen of a much larger optical depth (upper arrow) rather than altering the continuum slope as we do here. With regard to the continuum subtraction procedure, the effect of the homogeneous model is ~ 0.5 dex (factor 3) smaller than the screen model.

Since the above quoted evidence suggests $A_V = 3^m$ to 4^m for either nucleus, an extinction *difference* between the nuclei appreciably exceeding $\Delta A_V = 1^m$ is unlikely. Even after applying $\Delta A_V = 1^m$ for both the continuum correction and an additional correction of the line ratios for an extinguishing screen, the intrinsic line ratios of A1 do not reach the LINER regime but are rather either Seyfert like or consistent with those of a high-excitation HII region.

Enforcing lower excitation at one place in the image has to be matched by higher excitation somewhere else – either in the extended emission or in B1 – because the normalization with reference to the LINER-like FW79 spectrum has to be upheld. Since published groundbased spectra taken with photoelectric devices from the central region show LINER-like line ratios (FW79, Fried & Ulrich 1985, Rieke et al. 1985, Morris & Ward 1988, Armus et al. 1989, Keel 1990, Veilleux et al. 1995) it is unlikely that *all* compact components radiate significantly higher excited spectra. Hence high excitation as found here in A1 can only occur as a local effect on a subarcsecond scale.

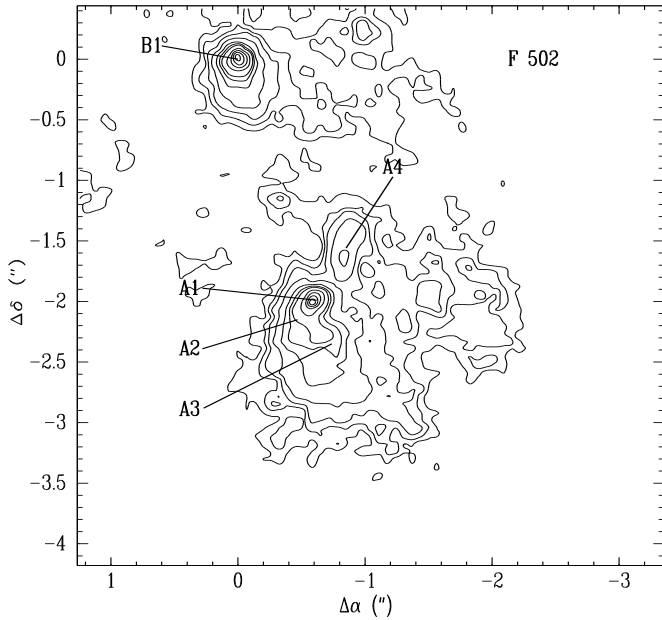


Fig. 6. Zoom from Fig. 3 showing the structure of the nuclei through F502M. Component A4 shows up most clearly in this frame

Comparing the measured line fluxes in $0''.26$ apertures with those in $0''.88$ apertures (=100%) centered on A1, we note that the smaller aperture contains 39% of $[\text{OIII}]+\text{H}\beta$, but only 3.8% of $[\text{OII}]$ which confirms that high excitation is *concentrated* in A1.

Even though our ignorance about the small-scale distribution of extinction hampers the derivation of reliable line ratios it is clear that, if there is low extinction in A1, *very high* excitation is inescapable; even in case of an unplausibly high extinction correction a *rather high* (AGN like) $[\text{OIII}]/[\text{OII}]$ value is still left for A1.

6. Discussion

The major finding from the new FOC data is that the southern nucleus, and especially its strongest component A1, is significantly higher excited than the northern compact component B1. How much does A1 contribute to the flux? To get a rough *relative* estimate of the *apparent* flux we ignore any extinction or continuum correction and obtain from Table 1 and $5007/\text{H}\beta \approx 10$ (cf. Sect. 5.1) $f(\text{H}\beta) = 1.17 \cdot 10^{-15} \text{ erg cm}^{-2} \text{ s}^{-1}$ for A1 ($0''.36$ aperture) which is $\sim 7\%$ of FW79's uncorrected $f(\text{H}\beta) = 1.7 \cdot 10^{-14} \text{ erg cm}^{-2} \text{ s}^{-1}$ ($3'' \times 6''$). Hence, what we see from the high-excitation source is inconspicuous. But what accounts for the high excitation: (i) a hidden AGN, (ii) a young stellar population, or (iii) fast shocks with precursor?

A hidden AGN. The best available evidence for an obscured AGN in NGC 6240 comes from ASCA X-ray data because they strongly resemble those of the hidden Seyfert-1 NGC 1068 (Mitsuda 1995). Also, two compact radio cores, each equivalent to $3 \cdot 10^5$ Cas A supernova remnants, may be considered as too extreme for an alternative starburst picture. If an AGN continuum

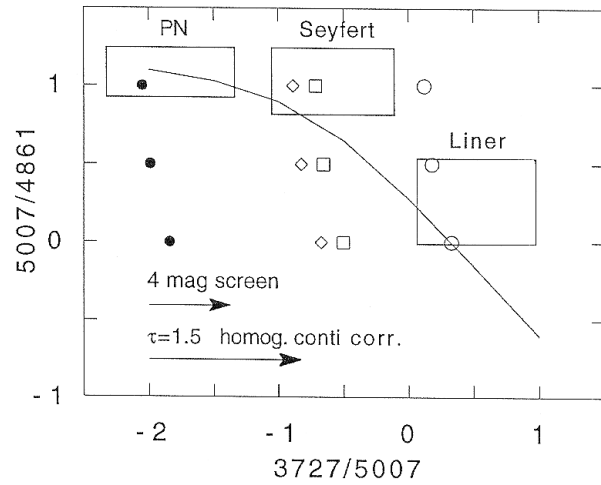


Fig. 7. Diagnostic diagram showing the logarithms of the intensity ratios $[\text{OIII}]\lambda 5007/\text{H}\beta$ versus $[\text{OII}]\lambda\lambda 3726, 29/[\text{OIII}]\lambda 5007$. The curve shows the mean loci of HII regions and planetary nebulae while the boxes give the regions where planetary nebulae, Seyferts and LINERs lie in this diagram. Data are given for the compact regions A1 (fat dots), A4 (diamonds), A3 (open squares) and B1 (open circles) and a circular aperture of $0''.26$ diameter. The three data points for each region correspond to the three assumed values of $[\text{OIII}]/\text{H}\beta$ (cf. Sect. 5.1). The small arrow gives the shift for a *directly* extinguishing screen with $A_V = 4^m$ with no change in the continuum subtraction procedure. The large arrow gives the shift for extinction model (iii) of Fig. 8 (cf. Sect. 5.2) (an additional small shift in $[\text{OIII}]/\text{H}\beta$ is neglected) which includes a reddening-corrected continuum subtraction procedure

ionizes A1 there should be an optically thin tunnel in the ISM between the hidden AGN source because the dominating circumnuclear low-ionization gas is unlikely to be ionized by the same source.

A young starburst. Prior to this work, clues from the ground-based optical or near infrared appear to be broadly consistent with an old background stellar population plus an ‘aged’ starburst dominated by stars of relatively low mass (Tanaka et al. 1991; Prestwich et al. 1994; Schmitt et al. 1996). An evolved burst explains the deficit in ionizing photons (counted from $\text{H}\beta$ or IR recombination lines) relative to the FIR luminosity. Looking for a stellar explanation, the extreme nature of the central radio sources might arise from overlapping bubble forming supernova remnants or extremely young remnants as was suggested by Colbert et al. (1994). Interpreting A1 as a localized high-excitation HII region with $L(\text{H}\beta) = 4\pi d^2 f(\text{H}\beta) = 1.3 \cdot 10^{39} \text{ erg s}^{-1}$ requires $2.7 \cdot 10^{51} \text{ s}^{-1}$ H-ionizing photons. The stellar sources may not necessarily be hidden because OB stars accounting for the observed U continuum of A1 (see paper I and $M(U)$ in Table 1) could supply up to $1.5 \cdot 10^{52} \text{ cm}^{-1}$ ionizing photons. Although the absolute numbers are too small this conclusion is relatively robust because a reddening correction is likely to boost the continuum estimate more than the line photons.

Shock regions with precursor. The overall LINER-like emission-line spectrum, infrared H_2 lines, line widths of $\sim 10^3$

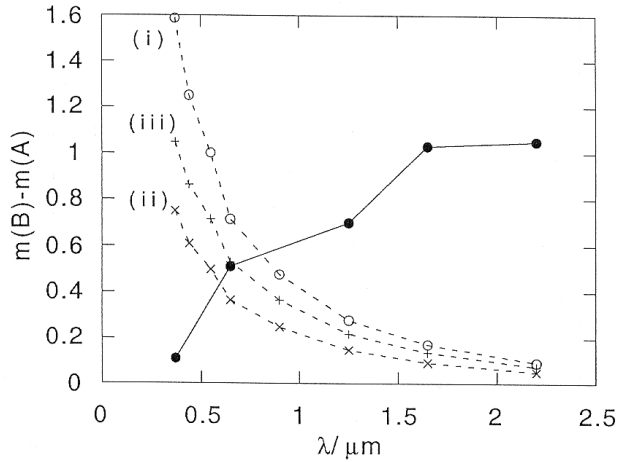


Fig. 8. The brightness difference of the two nuclei from the U band to the K band (measured with a $1''$ aperture by Thronson et al. 1990) plotted together with three different extinction geometries: (i) a model with an absorbing screen of $A_V = 1^m$; stars distributed in a homogeneous slab of absorbing material with either $\tau_V = 1$ (ii) or $\tau_V = 1.5$ (iii)

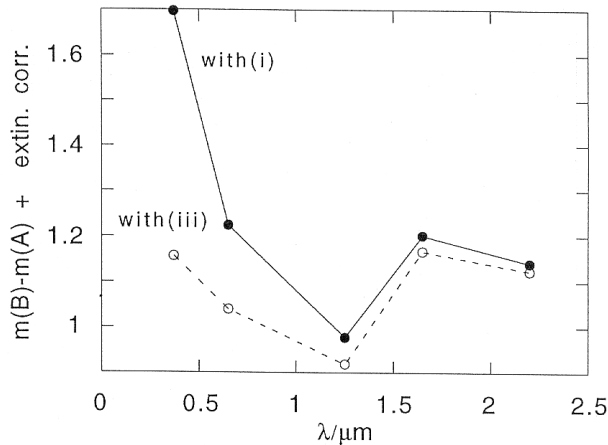


Fig. 9. The brightness difference between the nuclei after applying models (i) and (iii) of Fig. 8

km s^{-1} as well as the morphology favor shock-heating (e.g. Fried & Schulz 1983, Rieke et al. 1985, Armus et al. 1989; Keel 1990; van der Werf et al. 1993). If true for the low-ionization plasma, might shock heating also explain the high-excitation core A1? Recently, Dopita & Sutherland (1995) presented synthetic spectra from regions of *fast* shocks that include a precursor HII region, which is photoionized by EUV photons produced in the hot postshock plasma. With increasing shock velocity, these models would cover the region from LINERs well into the Seyfert range in our Fig. 7 (cf. their Fig. 1). Models *without* a precursor would lie in the LINER range (or below). We conclude that our continuum-corrected A1 data (or uncorrected data for A3 and A4) would fit shock+precursor models for velocities of about $300\text{--}500 \text{ km s}^{-1}$.

7. Summarizing conclusions

In three different wavelength ranges (around 3700, 4300 and 5000 \AA) the two apparent nuclei seen from the ground have been decomposed into compact features down to the resolution limit of about $0''.1$ and extended emission on the arcsec scale.

After emphasizing the difficulties of a separation of the line fluxes from the underlying continua that is hampered by the likely occurrence of patchy extinction, we obtain plausible limits on the $[\text{OII}]/[\text{OIII}]$ and $[\text{OIII}]/\text{H}\beta$ line intensity ratios. They signify ranges from LINER like to HII-region like for most compact features except for the brightest knot A1 in the southern nucleus that indicates a very high excitation level even after a relatively extreme extinction correction.

Hence, assuming direct photoionization, A1 appears to be either related to a hidden AGN source or a young cluster of massive stars. However, A1 only shows $\sim 7\%$ of the recombination line flux in the central $3'' \times 6''$ of NGC 6240. A third possibility would be shock heating in the vein of recent models for autoionized shocked regions advanced by Dopita & Sutherland (1995). This appears attractive in view of other evidence for a prevalent role of shocks in NGC 6240. More stringent diagnostics of the ionizing agent requires high-spatial-resolution spectroscopy (e.g. with HST).

Acknowledgements. Italian and German VIGONI travel grants enabled part of the calibration work to be carried out. H.S. was supported by DARA under contract 50 OR 9102 8. P.R. is grateful to the Humboldt Stiftung for supporting a Visiting Professorship at AIP in Potsdam and to Prof. G. Hasinger for his hospitality. We thank Hans-Martin Adorf for help with the data reductions in the early stages of this work. This research has made use of the NASA/IPAC extragalactic database (NED) which is operated by the Jet Propulsion Laboratory, Caltech, under contract with the National Aeronautics and Space Administration.

References

- Armus, L. et al. 1989, ApJ, 347, 727
- Baldwin, J.A. et al. 1981, PASP, 93, 5
- Barbieri, C. et al. 1993, A&A, 273, 1 (paper I)
- Colbert, E.J.M. et al., 1994, ApJ, 436, 89
- DePoy, D.L. et al. 1986, ApJ, 307, 116
- Dopita, M.A., Sutherland, R.S., 1995, ApJ, 455, 468
- Draine, B.T., 1989, Proc. 22d ESLAB Symp., ed. B.H. Kaldeich (Paris:ESA), p. 93
- Fosbury, R.A.E., Wall, J.V., 1979, MNRAS, 189, 79 (FW79)
- Fried, J., Schulz, H., 1983, A&A, 118, 166
- Fried, J., Ulrich, H., 1985, A&A, 152, L14
- Harwit, M. et al. 1987, ApJ, 315, 28
- Herbst, T.M. et al., 1990, AJ, 99, 1773
- Joseph, R.D. et al., 1984, MNRAS, 209, 111
- Joseph, R.D., Wright, G.S., 1985, MNRAS, 209, 111
- Keel, W.C., 1990, AJ, 100, 356
- Mitsuda, K., 1995, Ann.N.Y.Acad.Sc., 759, Proc. 17th Texas Symp. Relat. Ap. and Cosm., eds. H.Böhringer, G.E.Morfill, J.E.Trümper (New York: The New York Acad. of Sc.), p. 213
- Morris, S.L., Ward, M.J., 1988, MNRAS, 230, 639
- Lucy, L.B., 1974, AJ, 79, 745
- Paresce, F., 1990, Faint Object Camera Instrument Handbook, Version 2 (Baltimore: STScI and Noordwijk: ESA)

- Prestwich, A.H. et al., 1994, *ApJ*, 422, 73
Rieke, G.H. et al. 1985, *ApJ*, 290, 116
Sanders, D.B. et al. 1988, *ApJ*, 325, 74
Schmitt, H.R., Bica, E., Pastoriza, M.G., 1996, *MNRAS*, 278, 965
Schulz, H. et al., 1993, *A&A*, 277, 416 (erratum *A&A*, 284, 710, 1994)
Tanaka, M. et al., 1991, *ApJ*, 374, 516
Thronson, H. et al., 1990, *ApJ*, 364, 456
van der Werf, P.P. et al., 1993, *ApJ*, 405, 522
Veilleux, S., et al., 1995, *ApJS*, 98, 171
Wright, G.S. et al., 1984, *Nat*, 309, 430
Wynn-Williams, C.G., Becklin, E.E., 1993, *ApJ*, 412, 535
Zwicky, F. et al., 1961, *Catalogue of Galaxies and of Clusters of Galaxies I*, CalTech